American Mineralogist, Volume 78, pages 619–626, 1993

Structural modulation in sartorite: An electron microscope study

Allan Pring
Department of Mineralogy, South Australian Museum, North Terrace, Adelaide, South Australia 5000, Australia
Tim Williams
C.S.I.R.O. Division of Materials Science and Technology, Locked Bag 33, Clayton, Victoria 3168, Australia
Ray Withers
Research School of Chemistry, Australian National University, G.P.O. Box 4, Canberra, A.C.T. 2600, Australia

Abstract

Sartorite, $PbAs_2S_4$, has been examined by transmission electron microscopy. The mineral has a monoclinic (but metrically orthorhombic) subcell with $a = 19.62$, $b = 7.89$, $c = 4.19$ Å, $\beta = 90°$, and space group $P2_1/n$. In addition to the strong substructure reflections, **G**, corresponding to this monoclinic subcell, it also exhibits satellite reflections (in general incommensurate with respect to the subcell reflections) at $\mathbf{G} \pm m\mathbf{q}$, where m is an integer and **q**, the primary modulation wave vector ~6/13 (101)*. Some variation in the direction of the primary modulation wave vector was observed with the direction of the modulation being rotated up to 3° away from (101)* toward (001)*. Crystals with twin-related superlattices were also observed. Superlattice formation in sartorite is believed to result primarily from modulations in the lengths of arsenic sulfide chains within the structure.

Introduction

Sartorite is one of the lead arsenic sulfide minerals found in the dolomite at the unique deposit at Lengenbach, Binntal, Switzerland (Graeser, 1968, 1977). The mineral was first described under the name scleroclase by Walterhausen in 1857, and subsequently Dana proposed the name sartorite, for Sartorius Walterhausen, and this has gained general acceptance among English-speaking mineralogists (Palache et al., 1944). The simple stoichiometry of sartorite, $PbAs_2S_4$, belies the complexity of its crystallographic relations and structure. Early morphological crystallographers (Baumhauer, 1895; Solly and Jackson, 1902; Trechmann, 1907) failed to find a consistent set of axial ratios that would satisfactorily index all the observed forms. Smith and Solly (1919) extensively reviewed and repeated much of the earlier work and concluded that their crystals were composed of three lattices: one monoclinic and the others triclinic. X-ray diffraction studies by Bannister et al. (1939) showed the mineral to be monoclinic but with a strong orthorhombic subcell, $a = 19.46$, $b = 7.79$, $c = 4.17$ Å with a $3a \times b \times 20c$ supercell, i.e., $a' = 58.38$, $b' = 7.79$, $c' = 83.30$ Å, $\beta = 90°$. Using their data, Bannister et al. were able to assign indices to all forms reported in the morphological studies.

Nowacki et al. (1961) confirmed the orthorhombic subcell: their cell was $a = 19.62$, $b = 7.89$, $c = 4.19$ Å. They, however, found a $3a \times b \times 11c$ monoclinic supercell. Nowacki et al. (1961) solved and refined the structure of the subcell unit in the monoclinic space group $P12_1/n1$ [space group no. 14, unique axis b, cell choice 2 (Hahn, 1983)] with $\beta = 90°$, but they did not attempt to solve the superstructure. Note that the standard space group setting of $P12_1/c1$ (space group no. 14, unique axis b, cell choice 1) would require a redefinition of the unit-cell translations as follows: $\mathbf{a}' = \mathbf{c}$, $\mathbf{b}' = \mathbf{b}$, $\mathbf{c}' = -(\mathbf{a} + \mathbf{c})$, which would change β from 90 to 102.05°. Given the parent orthorhombic subcell symmetry of *Pbnm*, $a = 19.62$, $b = 7.89$, $c = 4.19$ Å, however, it would be inappropriate to reset the cell into this standard setting.

Iitaka and Nowacki (1961) further refined the structure, but not to their complete satisfaction. They curtailed their refinement at $R = 14.7\%$, leaving several aspects of the structure unclear, most notably the exact nature of the As_2S_3 chains running along the [001] direction. In particular, the bonds around the As atoms in the arsenic-sulfide chains are too long. Given the markedly large B_{33} temperature factors found for S2, S3, and S4 in their refinement, they concluded that the modulation was probably associated with some of the S atoms being displaced toward the As atoms along the **c** axis, thereby dividing the chains into finite lengths. In view of the large B_{11} temperature factor found for the Pb atoms, they also suggested that the Pb atoms might be displaced along the **a** axis so as to fill up the gaps left by the displacement of the S atoms.

Their subcell structure is shown in Figure 1. It can be considered as being composed of two structural elements: corner-sharing chains of PbS_9 tricapped trigonal prisms and layers of arsenic sulfide. The PbS_9 chains are similar to those in $PbCl_2$ (C23 structure) whereas the layers can be considered as slabs of distorted structures similar to GeS and α-SnS (B16 and B29 structure) (AsS slabs) with the coordination of the As being distorted from octahe-

0003–004X/93/0506–0619$02.00

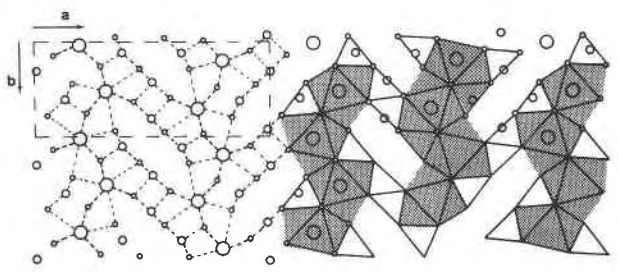

Fig. 1. Schematic diagram of the sartorite structure showing the chains of PbS_9 polyhedra parallel to **b**, which are cross-linked by strips of AsS_5 polyhedra in a twinned or zig-zag arrangement. The PbS_9 chains, similar to those found in $PbCl_2$, are shaded. The structure is viewed down [001]. Pb, large circles; As, medium circles; S, small circles.

dral to square pyramidal. The AsS slabs in sartorite are three AsS_5 polyhedra wide and are arranged around the PbS_9 chains.

We undertook this reinvestigation of the structure of sartorite by HRTEM and electron diffraction in order to clarify the nature of the sartorite structure and in particular the superstructure. This study is part of a wider reexamination of the structures of the lead arsenic sulfide minerals by high-resolution electron microscopy (Pring, 1990; Pring et al., 1990; Williams and Pring, 1988).

Experimental methods

Crystals of sartorite from Lengenbach, Binntal, Switzerland, were obtained from the collections of the South Australian Museum, Adelaide, the Department of Earth Sciences, University of Cambridge, and the Natural History Museum, Bern. For examination in the electron microscope, crystals or crystal fragments were ground under an organic solvent in an agate mortar and dispersed on Cu grids coated with holey carbon support films. The fragments were examined in several transmission microscopes, but mainly in a 200-kV Jeol 200CX and in a 300-kV Philips EM430 and a 300-kV CM30. (The 300-kV instruments have theoretical point-to-point resolutions in the range 2.3–~2.8 Å.) Additional electron diffraction studies were undertaken using tilt-rotate goniometers in Jeol 120CX and 100CX electron microscopes. Electron diffraction patterns were calibrated by vapor deposition of a thin coating of Au (~200 Å) onto the support films.

Results

Figure 2 shows an electron diffraction pattern and a lattice image from the [001] zone. This zone corresponds to the projection of the structure shown in Figure 1. The electron diffraction pattern (Fig. 2) shows an orthogonal 1/19.6 × 1/7.9 $Å^{-1}$ net with no apparent systematic absences evident along **b***. The space group suggested for sartorite, $P12_1/n1$ (Nowacki et al., 1961), requires absences for $0k0$, $k = 2n + 1$, and $h0l$, $h + l = 2n + 1$. The presence of the $0k0$, $k = 2n + 1$, forbidden reflections in Figure 2 is due to dynamical diffraction, as is clear from diffraction patterns when only the $0k0$ systematic row diffracts. The diffraction pattern and image show no evidence of supercell ordering or structural modulation in this zone.

An electron diffraction pattern from the [010] zone (Fig. 3) shows a 1/19.6 × 1/4.2 $Å^{-1}$ net with systematic absences $h0l$, $h + l = 2n + 1$, which are consistent with an n glide plane. The diffraction pattern also shows rows of sharp superlattice or satellite reflections parallel to (101)*: in terms of the reciprocal sublattice, the period of the superlattice is 1/13(101)*. Note that the satellite reflections at 6/13(101)* and 7/13(101)* are very strong, comparable in intensity in this electron diffraction pattern to the subcell reflections. In the language of modulated structures, these strong superlattice reflections represent the primary harmonic of an (in general) incommensurately modulated displacive modulation (see, for example, Perez-Mato et al., 1987). The strong superlattice reflections are at $\mathbf{G} \pm \mathbf{q}^{prim}$ with $\mathbf{q}^{prim} = 6/13(101)^*$, and this corresponds to a real space period of 8.8 Å. The other superlattice reflections [1/13(101)*, 2/13(101)*. . . .] are higher order harmonics (m) of $\mathbf{q}^{prim}$ and are labeled appropriately in Figure 3.

In general, a displacively modulated incommensurate structure can be described in terms of an underlying parent structure (in this case the $P2_1/n$ substructure, which gives rise to the set of strong subcell Bragg reflections, **G**) in combination with a displacive modulation field $\mathbf{u}_\mu(\mathbf{T})$ describing the structural deviation of the μth atom in the Tth parent unit cell away from its position in the underlying parent structure (see Perez-Mato et al., 1987; Withers, 1989; for discussion of nomenclature). In the case of a one-dimensionally modulated structure this atomic displacement field can be written in the form of a Fourier series as follows: $\mathbf{u}_\mu(\mathbf{T}) = \mathrm{Re}\,\Sigma\,\mathbf{e}_\mu(m\mathbf{q}^{prim})\exp(2\pi\,\mathrm{im}\,\mathbf{q}^{prim}\mathbf{T})$ where $m = 0, 1, 2, 3, \ldots$. A simple sinusoidal modulation would have zero eigenvector amplitudes $[\mathbf{e}_\mu(m\mathbf{q}^{prim})]$ for all except the first harmonics, i.e., for all except $m = 1$. In general, however, the possibility of an anharmonic modulation function must be allowed for, i.e., nonzero $\mathbf{e}_\mu(m\mathbf{q}^{prim})$ for $m > 1$.

The observation of higher order satellite reflections (at $\mathbf{G} \pm m\mathbf{q}^{prim}$) in electron diffraction patterns need not necessarily imply the existence of a genuine displacive modulation with a wave vector characterized by the corresponding modulation wave vector $m\mathbf{q}^{prim}$. In addition to the possibility of $\mathbf{G} \pm m\mathbf{q}^{prim}$ satellite reflections arising as a result of multiple diffraction, it is also possible that the reflections arise as a result of lower order modulation harmonics (see, for example, Withers et al., 1989). This is because a displacive modulation with modulation wave vector $\mathbf{q}$ gives rise to satellite reflections, not only at $\mathbf{G} \pm \mathbf{q}$, but also at $\mathbf{G} \pm m\mathbf{q}$, where m is an integer.

The diffraction pattern symmetry observed for sartorite requires the modulated structure to have a superspace group symmetry of $P{:}P2_1/n{:}-1,1$. This is a consequence of the superspace group satellite extinction condition $F(h, 0, l, m) = F(h\mathbf{a}^* + 0\mathbf{b}^* + l\mathbf{c}^* + m\mathbf{q}^{prim}) = 0$, unless $h +$

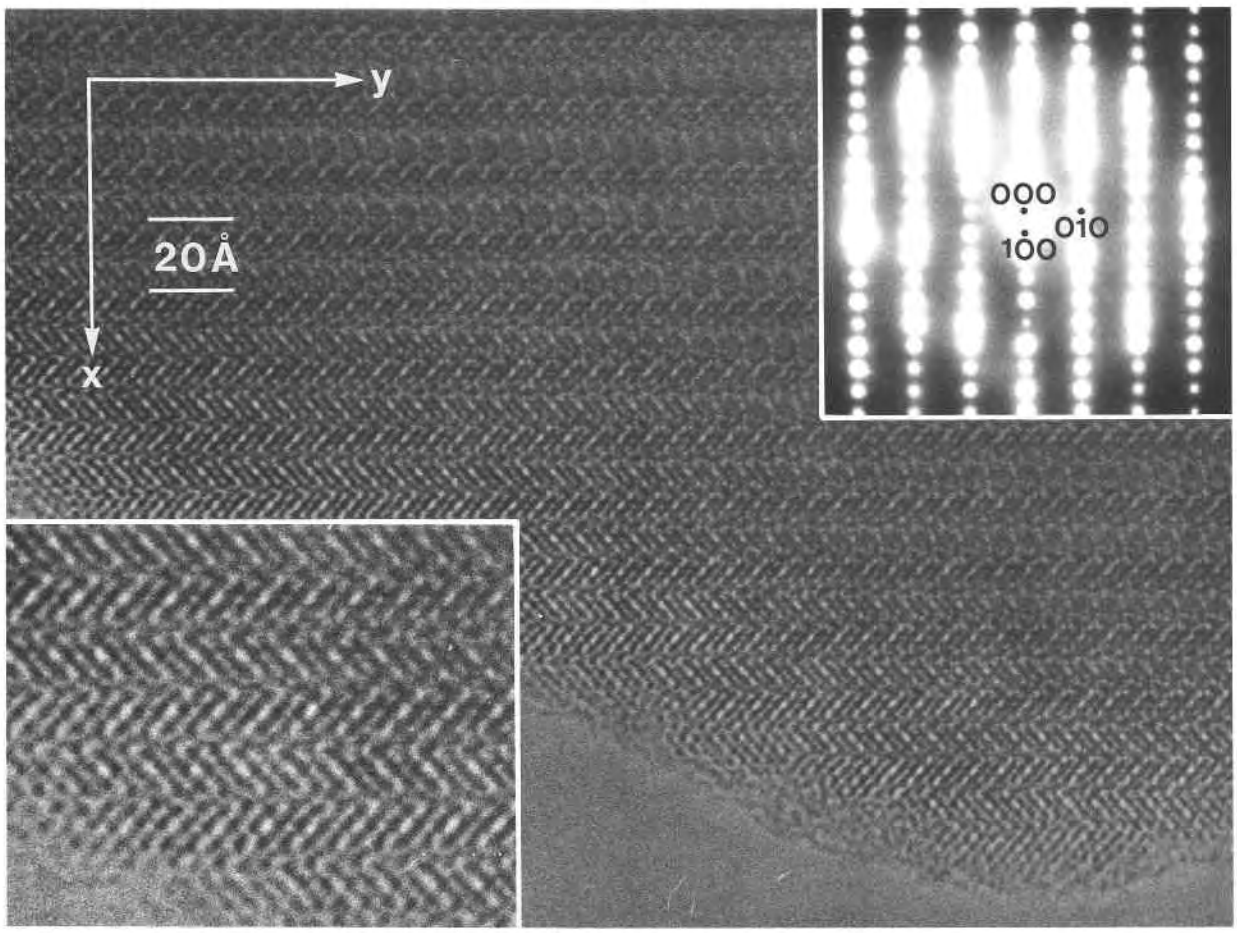

Fig. 2. Sartorite down the [001] zone. The electron diffraction pattern shows no superlattice or satellite reflections along either **a** or **b**. Magnified lattice image shows the zig-zag arrangement of the As-S layers that run between PbS layers. This view of the structure corresponds to that shown in Fig. 1.

$l = 2n$. De Wolff et al. (1981) provides a summary of notation and a listing of possible superspace groups. Note, however, that $P{:}P2_1/n{:}-1,1$ is not listed therein, as our choice of parent cell is not in the standard setting. The only possible alternative superspace group ($P{:}P2_1/n{:}-1,s$) implies the satellite extinction condition $F(h, 0, l, m) = F(h\mathbf{a}^* + 0\mathbf{b}^* + l\mathbf{c}^* + m\mathbf{q}^{prim}) = 0$, unless $h + l + m = 2n$, and this is clearly incompatible with experimental observations. The superspace group symmetry operation $\{\sigma_y | \frac{1}{2}(\mathbf{a} + \mathbf{b} + \mathbf{c}), -2\pi\mathbf{q}^{prim} \cdot \frac{1}{2}(\mathbf{a} + \mathbf{b} + \mathbf{c})\}$ constrains the form of the above atomic displacement field (see Perez-Mato et al., 1987, for a discussion of the constraints placed upon the atomic displacement pattern because of such superspace group symmetry operations). Further consideration, however, is beyond the scope of this paper.

In the pattern shown in Figure 3, the primary modulation wave vector is locked into rational values of the subcell repeat along (101)*. However, this is not always the case. Both the direction and period of the superlattice vary somewhat between different sartorite crystal fragments. However, it is possible to analyze these diffraction

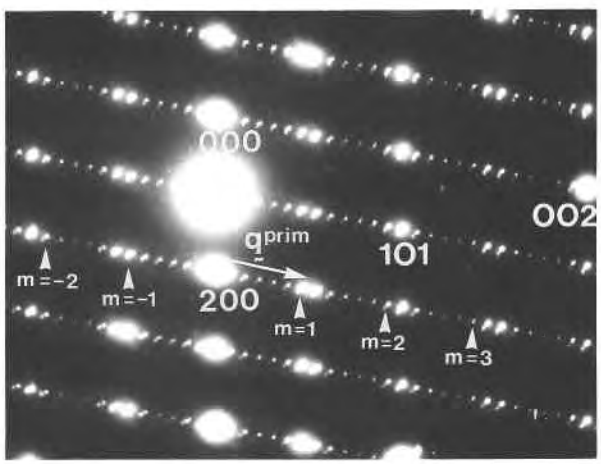

Fig. 3. The [010] electron diffraction pattern with rows of 13 sharp satellite reflections running along (101)*. Note that the satellite reflections 6/13(101)* and 7/13(101)* are very strong. These satellite reflections represent the primary modulation vector $\mathbf{G} \pm \mathbf{q}^{prim}$ with $\mathbf{q}^{prim}$ defined as 6/13(101)*. The higher order harmonics ($m = 2, 3, \ldots$) of $\mathbf{q}^{prim}$ are indicated.

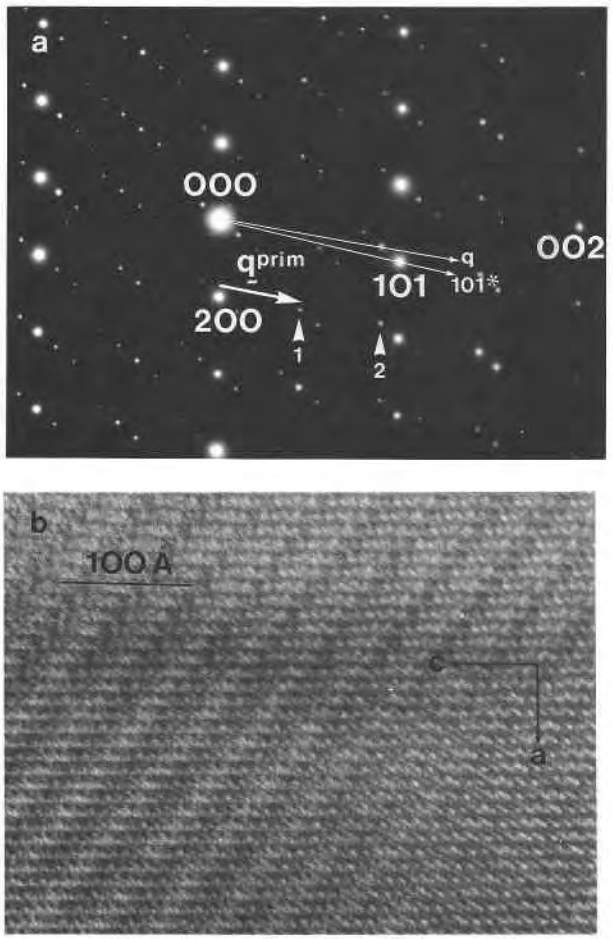

Fig. 4. Electron diffraction pattern and lattice image of sartorite taken down [010]. (**a**) The electron diffraction pattern shows an apparently incommensurate superlattice, which runs approximately along (15.0.4)* with a real space period of 32.4 Å. This pattern is generated by a rotation of $\mathbf{q}^{prim}$ 3° away from (101)* toward (001)*. The value of $\mathbf{q}^{prim}$ is again ≈6/13(101)*; the higher harmonics $m\mathbf{q}$ are labeled. (**b**) Corresponding lattice image showing contrast modulations due to the incommensurate modulation in the structure.

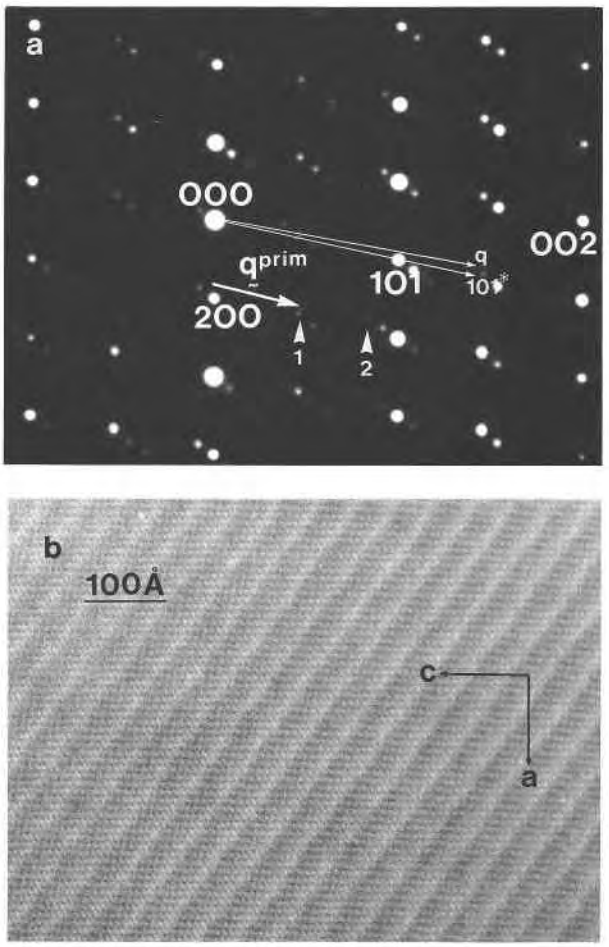

Fig. 5. Electron diffraction pattern and lattice image of sartorite taken down [010]. (**a**) The diffraction pattern shows rows of satellite reflections, which run approximately along (702)* with a period of ~40 Å. This superlattice is generated by rotating $\mathbf{q}^{prim}$ by 1.5° away from (101)* toward (001)*. The value of $\mathbf{q}^{prim}$ is ≈6/13(101)*, and the higher harmonics $m\mathbf{q}$ are labeled. (**b**) Lattice images showing the modulation in contrast due to the underlining strong harmonics of structural modulation.

patterns using the same $\mathbf{q}^{prim}$, but with small rotations of the vector from the $(101)^*_{sub}$ direction. Figures 4 and 5 show two [010] zone axis diffraction patterns and corresponding images in which both the period and direction of the superlattice modulation appear to have changed dramatically from the 13 × (101)* form shown above. The superlattice in Figure 4a appears to run approximately along (15.0.4)* with a period of ~32.4 Å, and that in Figure 5a approximately along (702)* with a period of ~40 Å. However, in both cases the superlattice can be treated as small rotations of $\mathbf{q}^{prim}$ away from (101)* toward (001)*. In Figures 4a and 5a, $\mathbf{q}^{prim}$ is rotated by 3 and 1.5°, respectively, toward (001)*; in both cases the higher order harmonics of $\mathbf{q}^{prim}$ are labeled on the diffraction patterns. The corresponding high-resolution lattice images (Figs. 4b, 5b) show strong contrast modulation due to the supercell, but in both cases there appears to be little variation in the underlying image motif of the substructure. The curved appearance of the superlattice fringes is due to the effects of increasing thickness on image detail. In all three examples of superlattices given above there is good lateral correlation in the modulation wave vector over the distances covered in these images. The lattice image in Figure 6 shows some irregularity in the superlattice fringes due to the partial breakdown of lateral correlation for the modulation. The corresponding electron diffraction pattern shows considerable canting and streaking of the superlattice reflections.

Two orientations of the primary wave modulation vector in a twin relationship occur in an appreciable number of crystals. Figure 7 shows an electron diffraction pattern with twinning of the primary modulation wave vector

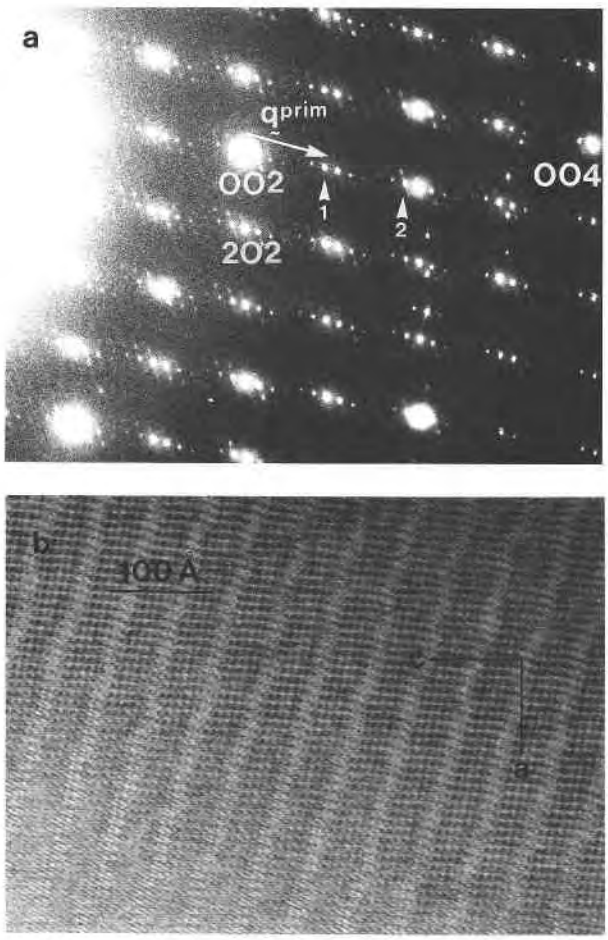

Fig. 6. Electron diffraction pattern and lattice image of sartorite taken down the [010] zone showing the effects of the breakdown in lateral correlation. (**a**) The electron diffraction pattern shows highly canted rows of superlattice reflections along (101)*. (**b**) Irregular fringes due to the breakdown in lateral correlation in the structural modulation.

across the (001) plane: the two directions of the wave vector are labeled. Slightly different rotations of $\mathbf{q}^{prim}$ and a breakdown in long-range lateral correlation can also be superimposed on the twinning, and the resulting [010] zone axis diffraction patterns can be very complex (see Fig. 8). Relations between superlattice reflections show that twinning is present, with domains up to several hundred ångströms across (see Fig. 9).

Finally, some single sartorite crystals appear to comprise an intergrowth of sartorite and another as yet unidentified, but closely related phase. In addition to sartorite patterns, which correspond to the 19.62 × 7.89 × 4.19 Å subcell, a number of diffraction patterns, all without superlattice reflections, were recorded from fragments derived from crushed single crystals. These second sets of diffraction patterns correspond to a phase with a 19.6 × 8.4 × 8 Å cell. The nature of this phase and its relationship to sartorite are yet to be fully established; however, it seems possible that it may be a polytype or polymorph of sartorite with a two-layer repeat structure (8.4 rather than 4.2 Å), possibly the sartorite II sample of Rösch and Hellner (1959).

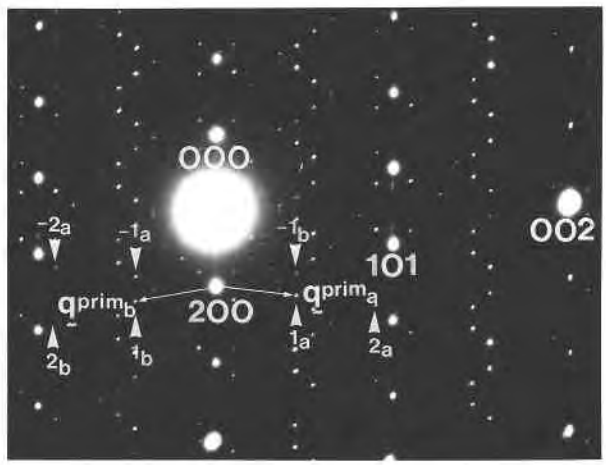

Fig. 7. Electron diffraction pattern down sartorite [010], showing satellite reflections due to twinned orientations of the structural modulation. The primary modulation vector ($\mathbf{q}^{prim}$) and the higher harmonics of both components are indicated. In both orientations $\mathbf{q}^{prim}$ is approximately 6/13(101)*, and it is rotated by 3° toward (001)* and away from (101)*. This pattern could be mistakenly interpreted as the $\sim 3a \times b \times 21c$ superlattice.

Discussion

The results of this study confirmed the subcell of sartorite to be orthorhombic; however, the superlattices observed do not correspond to either the $3a \times b \times 20c$ supercell of Bannister et al. (1939) or the $3a \times b \times 11c$ supercell of Nowacki et al. (1961). The satellite reflections occur along, or near to, the (101)* direction and not along either **a*** or **c***, except when twinning is present. It appears highly likely that the crystals examined by Bannister et al. (1939) and Nowacki et al. (1961) contained twinned forms of the structural modulation; the twins described above, for example, in Figures 7 and 8, can be interpreted as $\sim 3a \times b \times 21c$ and $\sim 4a \times b \times 13c$ superlattices, respectively. Given the experimentally observed slight variability in the primary modulation wave vector and the common occurrence of twinning, it would appear that both of the above reported superstructures could thereby be explained.

Because the twin relation is evident only in the weak, complex superlattice reflections, it is perhaps not surprising that Bannister et al. (1939) and Nowacki et al. (1961) were unsuccessful when they searched for evidence of twinning. The twinning noted in this work is ubiquitous, but on a very fine scale; the individual twin domains range in size from 50 to 5000 Å.

It is possible to consider the superlattices exhibited by sartorite as a family of superstructures with directions of the form $(h0l)$* and varying multiplicities, the directions

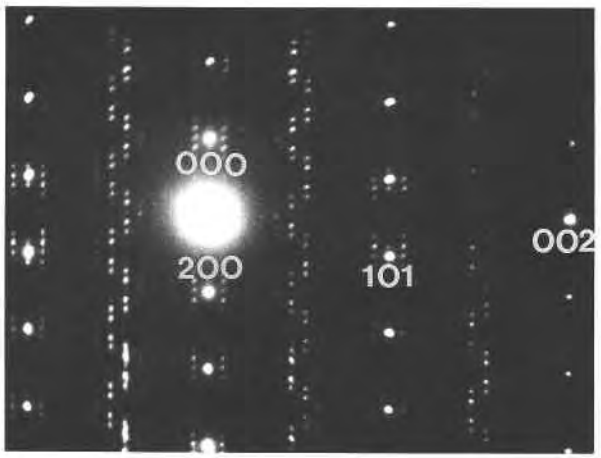

Fig. 8. Electron diffraction pattern down sartorite [010], showing satellite reflections due to twinning of the structural modulation. In this case, the modulations in the two components of the twin have rotated by slightly different amounts, and canting due to the breakdown in correlation is superimposed on the effects of twinning. This pattern could be mistakenly interpreted as $\sim 4a \times b \times 13c$ superlattice.

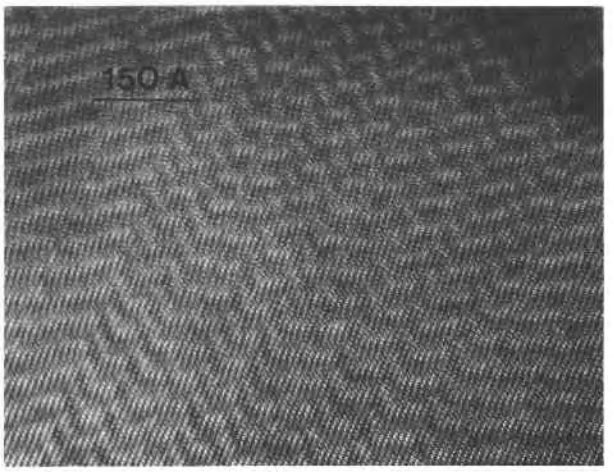

Fig. 9. Lattice image of sartorite down [010] showing domains of ordered twinning of the structural modulation, which range from 50 up to 150 Å in width.

of superstructure members observed here being (101)*, ~(702)*, and ~(15.0.4)*, which cover an angular range of ~35° and vary in periodicity from ~32.4 to ~53.3 Å. Such gross variation in direction and period would suggest major rearrangements of the parent substructure. However, the observed superlattice reflections can be considered in terms of an incommensurately modulated displacive modulation, with a common primary modulation wave vector $\mathbf{q}^{\text{prim}} = 6/13(101)^*$, which undergoes a series of small rotations. In each case a series of higher harmonics of the primary modulation wave vector is observed. This analysis suggests that only minor rearrangements of the parent substructure are required to produce the observed sets of diffraction patterns.

The origin of the structural modulation superlattices is a question of some importance, but unfortunately it is not possible to resolve this problem unequivocally on the basis of the electron diffraction and lattice image data, even with the aid of computer image simulations. Structural modulations can be either compositional or displacive in origin, and in the case of gross compositional modulation, a displacive component is also usually associated. Withers (1989) suggested that it is possible to distinguish between compositional and displacive modulations on the basis of the intensity distribution of the superlattice reflections. Thus, in the case of compositional modulation, the satellite reflections are strongest near the center of the diffraction pattern, whereas for a displacive modulation, the intensity of the satellite reflections initially increases as $|\mathbf{G}^* \pm m\mathbf{q}|$ increases, until the contribution of the temperature factor dominates, and the intensity decays. The intensity distribution in the satellite reflections in Figure 4a, the clearest of the diffraction patterns, suggests to us a displacive origin for the modulation. The fact that the underlying basic lattice motif does not appear to change in images from crystals exhibiting superlattices also suggests that the structural modulations are not compositional in origin. Iitaka and Nowacki (1961) suggested that the origin of the superlattice lay with variations in the arsenic-sulfur linkages. The bonds around the As in the arsenic-sulfide chains are too long, and the bridging S atoms exhibit exceptionally high thermal parameters along the chain directions.

Iitaka and Nowacki (1961) concluded that the S atoms were periodically displaced toward the As atoms, thus dividing the chains into finite lengths, and suggested that this process resulted in the formation of the superlattice. The direction of the structural modulation is normal to the {101} planes, and the displacements responsible for the modulation probably lie in or near the {101} planes. Figure 10 shows a view of the sartorite structure projected onto the {010} plane, with the As-S chains shown and some of the (101) planes traced. It can be seen that S atoms in the As-S chains lie just to either side of these planes. One possible model for the origin of the modulation, based on a longitudinal displacement, which is consistent with the structure refinement by Iitaka and Nowacki (1961), is that the S atoms that fail to bridge correctly are displaced toward the plane, as indicated in the diagram. This process leads to the subdivision of the As-S chain into segments two $[AsS_3]$ units in length. The Pb atoms might also be displaced along **a** so as to fill up the gap left by the displacement of the S atoms. The equivalence of the (101) and $(\bar{1}01)$ planes in the substructure provides a plausible explanation for the observed twinning. However, although this model is consistent with the structural data of Iitaka and Nowacki (1961), it must be stressed that it is only one of many possible models, and it is not possible with the available electron diffraction patterns and lattice images to establish the nature of the atomic displacements responsible for the structural

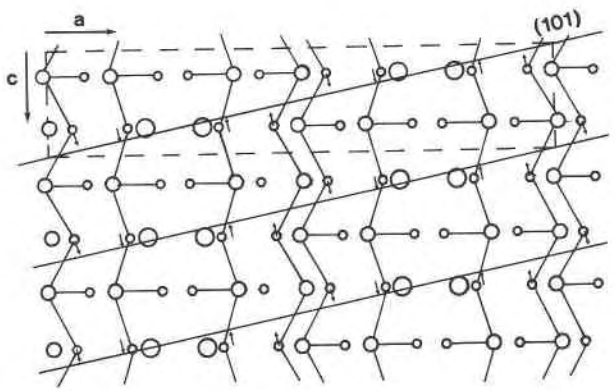

Fig. 10. Schematic structural diagram of the sartorite structure on (010), showing the atomic positions and traces of the {101} planes. The structural modulation is believed to be associated with the displacement of atoms in the AsS chains around the {101} planes. The AsS chains running parallel to [001] are divided into segments by displacements of the S atoms toward the (101) planes. (Pb, = large circles; As, medium circles; S, small circles.)

modulations. Lattice image simulations using the multislice method are not particularly sensitive to atomic displacements and do not offer a unique solution to the problem, especially given the number of variable parameters independent of the structure (e.g., thickness and defocus) that must also be established. With the aid of high-quality refinement of the structure, with single-crystal X-ray diffraction methods, it may be possible to fully resolve the nature of the modulated structure of sartorite.

A displacive origin for the modulated superstructure suggests that the mineral undergoes a displacive phase transition at higher temperature (cf. α-β cristobalite, α-β quartz: Hyde and Andersson, 1989). No such transitions have yet been reported in the Pb-As-S minerals. Kutoglu (1969) found that sartorite decomposes semicongruently to form baumhauerite and liquid at 305 °C. Attempts to initiate a transition by heating crystal fragments with the electron beam were made during this electron microscopy study but were unsuccessful. Decomposition occurs rapidly when a high-intensity electron beam is focused onto the fragment. A detailed investigation into the thermal behavior of sartorite would seem warranted.

It is interesting to note that the English morphological crystallographer H.G.F. Smith had trouble finding rational indices for sartorite (Smith and Solly, 1919) and experienced similar problems when studying calaverite (Smith, 1902). Recent studies of calaverite have shown that it also has a modulated structure (van Tendeloo et al., 1983; Schutte and de Boer, 1988). Whereas morphological crystallographers at the turn of the century were unaware of the existence of modulated structures, they were, by their careful measurements, able to detect that minerals such as sartorite and calaverite were crystallographically unusual. It may be possible to identify additional minerals with modulated structures by studying the works of the morphological crystallographers of the turn of the century.

Acknowledgments

We wish to thank the following people for giving us access to the transmission electron microscopes in their charge: D.A. Jefferson, Department of Physical Chemistry, University of Cambridge, J. Fitz Gerald, Research School of Earth Sciences, and B.G. Hyde, Research School of Chemistry, Australian National University, A. Johnson, Electron Optical Centre University of Western Australia, and P. Self, C.S.I.R.O. Division of Soils, Adelaide. The specimens in this study were provided by A. Stalder, Natural History Museum, Bern, and G. Chinner, Department of Earth Sciences, University of Cambridge. Stimulating discussions with B.G. Hyde helped shape our understanding of the nature of the sartorite structure. The financial assistance of the Australian Research Council to A.P. is gratefully acknowledged.

References cited

Bannister, F.A., Pabst, A., and Vaux, G. (1939) The crystallography of sartorite. Mineralogical Magazine, 25, 264–270.

Baumhauer, H. (1895) Über den skleroklas von Binn. Sitzungsberichte der Akademie der Wissenschaften, Berlin, 12, 243–252.

De Wolff, P.M., Janssen, T., and Janner, A. (1981) The superspace groups for incommensurate crystal structures with a one-dimensional modulation. Acta Crystallographica, A37, 625–636.

Graeser, S. (1968) Die Sulfosalze des Binntales: Geochemie und Genese. Jahrbuch, Naturhistorisches Museum der Stadt Bern, 1966–1968, 46–63.

——— (1977) Lengenbach, Switzerland. The Mineralogical Record, 8, 275–281.

Hahn, T., Ed. (1983) International tables for crystallography, vol. A, 119 p. Reidel, Dordrecht, Holland.

Hyde, B.G., and Andersson, S. (1989) Inorganic crystal structures, p. 392–397. Wiley Interscience, New York.

Iitaka, Y., and Nowacki, W. (1961) A refinement of the pseudo crystal structure of scleroclase $PbAs_2S_4$. Acta Crystallographica, 14, 1291–1292.

Kutoglu, A. (1969) Röntgenographische und thermische Untersuchungen im quasibinären System PbS-As2S3. Neues Jahrbuch für Mineralogie Monatshefte, 68–72.

Nowacki, W., Iitaka, Y., Burki, H., and Kunz, V. (1961) Structural investigations on sulfosalts from Lengenbach, Binn Valley, (Ct. Wallis), Part 2. Schweizerische mineralogische und petrographische Mitteilungen, 41, 103–116.

Palache, C., Berman, H., and Frondel, C. (1944) Dana's system of mineralogy (7th edition, vol. 1), p. 478–480. Wiley, New York.

Perez-Mato, G., Madariaga, G., Zuñiga, F.J., and Garcia Arribas, S.A. (1987) On the structure and symmetry of incommensurate phases. A practical formulation. Acta Crystallographica, A43, 216–226.

Pring, A. (1990) Disordered intergrowths in lead arsenic sulfide minerals and the paragenesis of the sartorite group minerals. American Mineralogist, 75, 289–294.

Pring, A., Birch, W.D., Sewell, D., Graeser, S., Edenharter, A., and Criddle, A. (1990) Baumhauerite-*2a*: A silver-bearing mineral with a baumhauerite-like supercell from Lengenbach, Switzerland. American Mineralogist, 75, 915–922.

Rösch, H., and Hellner, E. (1959) Hydrothermale Untersuchungen am System PbS-As_2S_3. Naturwissenschaften, 46, 72.

Schutte, W.J., and de Boer, J.L. (1988) Valence fluctuations in the incommensurately modulated structure of calaverite $AuTe_2$. Acta Crystallographica, B44, 486–494.

Smith, H.G.M. (1902) On the remarkable problem presented by the crystalline development of calaverite. Mineralogical Magazine, 13, 122–150.

Smith, H.G.M., and Solly, R.H. (1919) On sartorite and the problem with its crystal-form. Mineralogical Magazine, 18, 259–316.

Solly, R.H., and Jackson, B.A. (1902) Sulpharsenites of lead from Binnenthal. Mineralogical Magazine, 12, 282–297.

Trechmann, C.O. (1907) Crystallography of sartorite from Binn. Mineralogical Magazine, 14, 212–229.

Tendeloo, G., Gregoriades, P., and Amelinckx, S. (1983) Electron microscopy studies of modulated structures in (Au,Ag)Te_2. I. Journal of Solid State Chemistry, 50, 321–334.

Williams, T.B., and Pring, A. (1988) Structure of lengenbachite: A high-resolution transmission electron microscope study. American Mineralogist, 73, 1426–1433.

Withers, R.L. (1989) The characterization of modulated structures via their diffraction patterns. Progress in Crystal Growth and Characterization, 18, 139–204.

Withers, R.L., Wallenberg, R., Bevan, D.J.M., Thompson, J., and Hyde, B.G. (1989) The fluorite-related solid solutions of CeO2-Y2O3. II. A modulated structure approach. Journal of the Less-Common Metals, 156, 17–27.

Manuscript received February 3, 1992
Manuscript accepted January 6, 1993